NUMERICAL SIMULATION OF DYNAMIC FAULT RUPTURE PROPAGATION BASED ON A COMBINATION OF BIEM AND FEM SOLUTIONS

H. Goto[1], L. Ramírez-Guzmán[2] and J. Bielak[3]

[1] *Assistant Professor, Disaster Prevention Research Institute, Kyoto University, Kyoto, Japan*
[2] *Grad. Student, Dept. of Civil and Environmental Engineering, Carnegie Mellon University, Pittsburgh, USA*
[3] *Professor, Dept. of Civil and Environmental Engineering, Carnegie Mellon University, Pittsburgh, USA*
Email: goto@catfish.dpri.kyoto-u.ac.jp, lramirez@andrew.cmu.edu, jbielak@cmu.edu

ABSTRACT :

In recent years, dynamic source rupture models have been increasingly used to represent the fault rupture propagation during earthquakes. Several numerical approaches, such as the finite difference method, the finite element method and the boundary integral equation method, have been proposed for the numerical simulation of the rupture propagation. However, seldom do the proposed numerical simulation methods support both the accuracy of the stress field close to the fault surface and the representation of a complex heterogeneous media. For instance, boundary integral equation methods provide accurate stress field near the fault surface, stemming from the analytical fundamental solutions used in their formulation. Yet, these methods are generally applied to a simple homogeneous infinite medium due to the difficulty of determining the required fundamental solutions for more general media. On the other hand, while domain-based methods, such as the finite element method, are applicable to arbitrary complex media, the accuracy of the resulting stress field near the fault surface is low. We propose a new approach for analyzing the fault rupture propagation based on the combination of the boundary integral equation method (BIEM) and the finite element method (FEM) in order to capture the advantages of each approach. We apply it to simple half space problem in order to investigate the effects of the free surface on the fault rupture propagation in 2D P-SV problems.

KEYWORDS: Dynamic source rupture model, Rupture simulation, FEM, BIEM

1. INTRODUCTION

Dynamic source rupture models simulate a physically consistent slip distribution based on tectonic loadings, fault geometries, friction laws, material properties, etc. Three-dimensional simulations of historical earthquakes using dynamic source rupture models have led to a deeper understanding of physical aspects of the earthquake mechanics. In the simulation, the equation of motion is numerically solved by using either domain or boundary based methods. Domain based methods, such as finite difference methods (FDM) or finite element methods (FEM), are applicable to arbitrary geologic structures and fault geometries, but require a field discretization within the domain of interest. Its main difficulty is to accurately represent the stress tensor around the fault plane. In contrast, boundary based methods, such as the boundary integral equation method (BIEM), accurately resolve the stresses, but depend on the availability of the Green's function.

A field discontinuity in domain methods can be represented either explicitly as a surface whose nodes have double degrees of freedom, the Split Nodes (SN), or via an inelastic region that represents the fault, the Stress Glut (SG). The SN method in seismological applications was proposed and implemented in 2D FDM by Andrews (1973) and improved and analyzed by Day (1982), Virieux and Madariaga (1982), Kase and Day (2006), Miyatake and Kimura (2006) and Dalguer and Day(2007). In the context of FEM, Aagaard (1999) and Oglesby (2000a, 2000b) applied a similar concept in three-dimensions using low order finite elements. More recently, Festa (2004) used high order elements, known as spectral elements, with a nodal-integration technique to lump the mass, applied the split node approach to analyze the rupture. Stress Glut methods have been used in FDM and were proposed by Andrews (1976) and Madariaga *et al.*(1998) and analyzed in Dalguer and Day (2006). Due to the limitations of FDM, Cruz-Atienza and Virieux (2004) proposed SG approach to simulate rupture in complex geometries.

Kostrov (1966) first derived the time domain boundary integral equation for dynamic elastic problems, and Das (1980) extended it for 3D problems. Their formulations and related works, e.g. Das and Aki (1977a, 1977b), Andrews (1985, 1994) are based on the convolution of weak singular kernels and stress changes, which are described in Kostrov and Das (1989) and Aki and Richards (2002). However, their formulations are difficult to apply for arbitrary fault geometries because the integral kernels are constructed from the half space Green's function with free surface condition on the fault plane. Therefore, another representation of boundary integral equation, traction formulation, was developed. The boundary integral equation is based on the convolution of hyper-singular kernels and dislocations, and the treatment of hyper-singularity has been challenged. Sladek and Sladek (1984) and Nishimura and Kobayashi (1989) presented regularization technique for dynamic elastic problems, and Koller *et al.*(1992) introduced the regularizations into the dynamic rupture simulations. Their applications and the other improved BIE are those derived by Cochard and Madariaga (1994), Fukuyama and Madariaga (1995), Tada and Yamashita (1997), Fukuyama and Madariaga (1998), Tada *et al.*(2000). Recently, Goto and Bielak (2008) proposed a Galerkin BIE method for 2D SH problem, which results in more rapid convergence than the previous methods. Time domain BIE methods provide highly accurate solutions; however, the simulations are limited to simple full space problems. Spectral boundary integral equation method [e.g. Geubelle and Rice, 1995, Cochard and Rice, 1997, Lapusta *et al.*, 2000] is another approach with high order of convergence but is applicable to simple half space problems, which is explicitly mentioned in Zhang and Chen (2006a, 2006b). However, the applicable problems have still been limited.

Boundary based methods provide the accurate representation of stress change around the fault plane, although they are limited to simple problems. On the other hand, whereas domain based methods support complex geological structures, they require substantial numerical treatment on the fault plane. In this article, we propose a new technique which combines the advantages of boundary and domain based methods. We, then, analyze and speculate on the effect of the free surface as a feedback mechanism in the rupture process.

2. COMBINATION APPROACH OF BOUNDARY INTEGRAL EQUATION AND FINITE ELEMENT METHOD

Let S be a single planar fault embedded in an elastic 2D space V and x_1 and x_2 the axis of a Cartesian system along and perpendicular to the fault S, respectively. This paper discusses inplane cases consisting of shear slip displacements $\Delta u_1(x_1,t)$, which is parallel to the fault S, in the rupture propagation direction x_1 at time t. In general, the slip or jump is defined as,

$$\Delta u_1(x_1,t) = \lim_{\varepsilon\to+0}\left[u_1(x_1+\varepsilon,0,t) - u_1(x_1-\varepsilon,0,t)\right], \tag{2.1}$$

where $u_1(x_1,x_2,t)$ (i = 1, 2) is the displacement vector field. The jump in the displacements generates a traction change $\Delta T_1(x_1,t)$ on both, the hanging and foot walls of the source. Although applicable to tensile components of the traction, we focus on the shear traction changes parallel to the excited slip directions.

In the case of a homogeneous full space V^H, it can be shown [e.g. Tada and Yamashita, 1997] that the integral representation of the traction change given the slip, the Π^H boundary value problem, is:

$$\begin{aligned}\Delta T_1^H(x_1,t) = &-\frac{\mu}{2\beta}\Delta\dot{u}_1(x_1,t) - \frac{2\mu\beta^2}{\pi}\int_S \frac{1}{(x_1-\xi)^3}d\xi\int_0^t \frac{\partial\Delta\dot{u}_1(\xi,\tau)}{\partial\xi}(t-\tau)\sqrt{(t-\tau)^2 - r^2/\alpha^2}\,H(t-\tau-r/\alpha)d\tau \\ &+\frac{\mu\beta^2}{2\pi}\int_S \frac{1}{(x_1-\xi)^3}d\xi\int_0^t \frac{\partial\Delta\dot{u}_1(\xi,\tau)}{\partial\xi}\frac{\left[2(t-\tau)^2 - r^2/\beta^2\right]^2}{(t-\tau)\sqrt{(t-\tau)^2-r^2/\beta^2}}H(t-\tau-r/\beta)d\tau\end{aligned} \quad ,(2.2)$$

where $H(t)$ is Heaviside function, ξ is point on the fault where a unit load is applied, τ is instant at which the unit load is applied, $r = |x_1 - \xi|$, $\gamma_1 = (x_1 - \xi)/r$, μ is shear modulus, and α and β are P-wave velocity and S-wave velocity, respectively.

On the other hand, even though there are no general time domain analytical representations for inhomogeneous and/or bounded space V, the Π boundary value problem, we always can express ΔT as the sum of a reference traction from a Π^H problem plus a correction term ΔT^S,

$$\Delta T_1(x_1,t) = \Delta T_1^H(x_1,t) + \Delta T_1^S(x_1,t)\,. \tag{2.3}$$

Then, the term ΔT^S represents the additional effect due the inhomogeneities or boundary conditions, which we will refer throughout the document as the "scattered term". Since the later usually does not have time domain analytical boundary integral representation, we propose an algorithm to construct it utilizing two finite element realizations. The source is represented via localization of the displacements using a stress glut approach. The advantage of this choice is the versatility gained in the geometry of the fault; no mesh following the source is required.

A stress change at time t computed numerically using FEM, is a function of the discretization of the prescribed slip displacement $\Delta\bar{u}_1$. Then,

$$\Delta\bar{T}_1^{\text{hete}}(x_1,t) = F^{\text{hete}}[\Delta\bar{u}_1(x_1,t)]\,, \tag{2.4}$$

where F^{hete} represents the transformation on $\Delta\bar{u}_1$ associated to the FEM solution of Π. Even though the frequency range accurately represented can be accounted by the selection of the slip function, the field approximation order and the size of the elements, the tractions near the source are inaccurate; a discontinuity is artificially approximated by the SG.

Moreover, the traction change $\Delta\bar{T}_1^{\text{hete}}$ can also be divided into a "direct" or homogeneous $\Delta\bar{T}_1^H$ and scattered $\Delta\bar{T}_1^S$ tractions:

$$\Delta\bar{T}_1^{\text{hete}}(x_1,t) = \Delta\bar{T}_1^H(x_1,t) + \Delta\bar{T}_1^S(x_1,t)\,. \tag{2.5}$$

In order to extract the artificial discontinuity, we associate $\Delta\bar{T}_1^H$ to the numerical solution of a Π^H problem. Thus,

$$\Delta\bar{T}_1^{\text{homo}}(x_1,t) = F^{\text{homo}}[\Delta\bar{u}_1(x_1,t)] = \Delta\bar{T}_i^H(x_1,t)\,. \tag{2.6}$$

Therefore, the numerical scattered term $\Delta\bar{T}_1^S$ can be extracted from the two FEM solutions:

$$\Delta\bar{T}_1^S(x_1,t) = \Delta\bar{T}_1^{\text{hete}}(x_1,t) - \Delta\bar{T}_1^{\text{homo}}(x_1,t)\,. \tag{2.7}$$

The accuracy of Eqn.2.7 depends on the distance between the heterogeneous structures and the fault. If the fault lies away from the layer boundary or some inhomogeneities, the scattered term ΔT^S is approximated by its numerical counterpart:

$$\Delta T_1^S(x_1,t) \simeq \Delta\bar{T}_1^S(x_1,t)\,. \tag{2.8}$$

From Eqns.2.3, 2.7 and 2.8, we immediately can write the total traction change of the Π problem:

$$\Delta T_1(x_1,t) \simeq \Delta T_1^H(x_1,t) + \Delta \overline{T}_1^{\text{hete}}(x_1,t) - \Delta \overline{T}_1^{\text{homo}}(x_1,t)\,. \tag{2.9}$$

The left hand of Eqn.2.9 represents the shear traction change generated by slip displacement $\Delta u_1(x_1,t)$ in inhomogeneous, bounded space, layered and heterogeneous structures V, the Π problem. On the other hand, the right hand of Eqn.2.9 consists of three terms. The first term ΔT^H is the traction change represented by the analytical boundary integral equations (Eqn.2.2); this term is responsible for the accuracy of stress field near the fault plane. The second term is numerically calculated from FEM of the Π problem, which term represents the heterogeneity of the target medium. The third term is also numerically calculated from FEM of the Π^H problem; it extracts the scattered term. Eqn.2.9 supports an accurate representation of traction change beside a slip region on the order of that of the BIE, and also supports the effects of inhomogeneous and/or bounded space as the FEM. This characteristic satisfies the requirements of dynamic rupture simulation. Notice that, we do not need to select the contribution between BIE and FEM depending on the target region in the model, for example "source box" around the fault area. The contribution is automatically weighted based on Eqn.2.9.

3. SPONTANEOUS RUPTURE SIMULATION

3.1 Governing equations

Numerical simulation of spontaneous rupture propagation requires that the slip displacement and the traction change communicate at every instant t based on the governing equations. One of the governing equations is the friction law for the fault rupture. In the following expressions and numerical simulations, a slip-weakening friction law is applied because we just focus on the effectiveness of our proposed approach to the catastrophic rupture process, formulated as follows.

$$T_C - T_1 \geq 0, \qquad (T_C - T_1)\Delta \dot{u}_1 = 0\,. \tag{3.1}$$

where T is the absolute value of traction, f_1 and f_2 are the time-dependent coefficients to form the slip-weakening curve. The original representation of Eqn.3.1 is normalized by the compressive normal stress. However, we choose to work with the explicit values because the following numerical calculations do not generate compressive stress changes. In the numerical simulations, a simple slip-weakening friction law proposed by Ida (1972) is selected as follows.

$$T_C(t) = \begin{cases} -\dfrac{T_P - T_R}{D_C}\Delta u_1(t) + T_P & (\Delta u_1 < D_C) \\ \qquad\quad T_R & (\Delta u_1 \geq D_C) \end{cases}. \tag{3.2}$$

where T_P is the yield traction, T_R the residual traction and D_C the slip-weakening distance, which are the constants.

Another governing equation is the representation of traction related to the generated slip displacement on the source fault. The traction consists of an initial traction and the traction change excited by slip displacements.

$$T_1(t) = T_I + \Delta T_1(t)\,, \tag{3.3}$$

where T_I is the initial traction. As described in section 2, the traction change in Eqn.3.3 is the function of the slip displacement, and is calculated by the proposed approach Eqn.2.9 in the general space V.

3.2. Numerical model

Simple numerical simulations of spontaneous rupture propagation are performed. Figure 1 shows the target half space model, characterized by a P-wave velocity of 6000 m/s, S-wave velocity of 3464 m/s, and a density of

2670 kg/m^3. We consider four different angles of the fault: 0˚, 30˚, 60˚ and 90˚. The upper left side of the fault is located 1 km below the free surface, and the fault length is 10 km.

Governing parameters related to the simple slip-weakening law (Eqn.3.2) are T_P, T_R, D_C and the initial traction T_I. Asymmetric parameter model is simulated as shown in Figure 2. T_P and T_R are constant with 81.24 MPa and 63 MPa, respectively. High T_I is localized in 7500-8500 m with 81.6 MPa as the nucleation region, otherwise low T_I is distributed surrounding the nucleation region with 70 MPa. D_C distribution contains short D_C region with 0.4 m in 4000-10000 m and long D_C region with 1.0 m in 0-4000 m to restrain the rupture propagation.

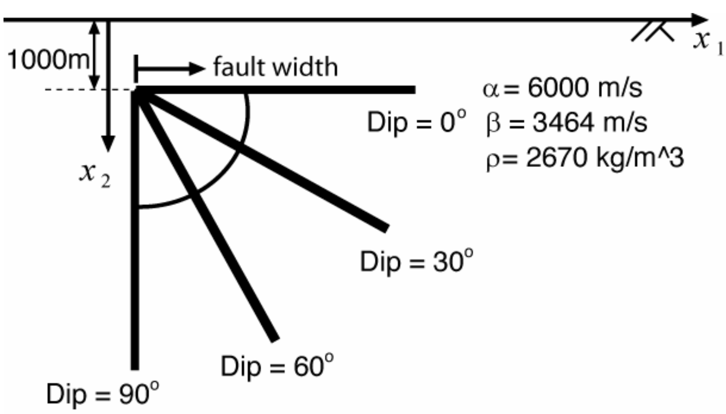

Figure 1 Geometry of numerical simulation in half space

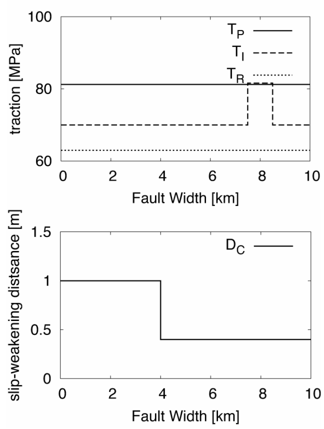

Figure 2 Fault parameter model for the spontaneous rupture simulation

3.3. Numerical simulation of spontaneous rupture propagations

Simple numerical tests for spontaneous rupture propagations are performed. 100 m square meshes for FEM calculation and 100 m line meshes for BIEM calculation are selected in the following simulations, respectively. Time step is selected as 0.0083 second to satisfy CFL=0.5.

We show simulated results of slip-rate and slip displacement time histories at 2 km, 3 km and 4 km on the fault in Figure 3. For the homogeneous full space case, the rupture stops at 2 km in the large D_C region. All half space cases can not stop the rupture in the large D_C region, and the time lag of the rupture start is presented for Dip 30˚, 60˚ and 90˚ cases. The rupture speed of Dip 0˚ case is faster than the other dip angle cases and the homogeneous full space case, and the final slip displacements increase with the lower dip angle cases. For Dip 30˚, 60˚, 90˚ cases, the peak time of the slip-rate appears just after the rupture start at 4 km, while the peaks delay at 2 km and 3 km. However, the peak time of Dip 0˚ case keeps just after the rupture start. This indicates the rupture driving energy is supplied by the scattered terms from the free surface, based on the consideration of energy balance. We mention that the selection of the dynamic parameters is arbitrary for the model simulation to control a rupture due to the scattered terms, while the scattered terms contain a potential to control the rupture propagation.

For Dip 30˚ case, snap shots of velocity field are plotted in Figure 4, and snap shots of velocity field in full space with full space rupture process are also plotted as a reference. Velocity field is represented by the absolute value of particle velocities. For the discussion, scattered Coulomb stress change are also plotted in Figure 4, which is the difference between the generated stress distributions simulated in half space FEM and ones in full space FEM. All the snap shots focus on 2.5-6.0 s in order to investigate the effects for the rupture propagation in the large D_C region. Positive Coulomb stress associated with the fault plane is the sense to trigger a rupture progress. Velocity field is symmetric distribution relative to the fault at 2.5 s, while the pattern gradually changes to be asymmetric. At the same time, we observe the generation of scattered Coulomb stress change around the free surface, and the phase propagates from the free surface to the fault. Once the scattered

Coulomb stress change reaches the fault surface, the rupture starts to propagate into the large D_C region and generate velocity wave field. After the rupture propagation, large velocities are observed between fault and free surface in 4.0-5.5 s.

Zhang and Chen (2006b) pointed out the possibility to accelerate the rupture speed of strike direction to super-shear rupture by the existence of free surface. In this paper, we just discuss the rupture propagation of dip direction, while the simulated results indicate the faster rupture speed is accelerated by the free surface. Zhang and Chen (2006b) also indicated that the rupture propagation in half space could not be controlled by the installed barrier represented by the high initial traction. Our simulation results with large D_C region represent similar characteristics. Oglesby *et al*. (2000a, 2000b) discussed the stronger ground motion in hanging wall by comparing the free surface effect for normal dipping fault and thrust dipping fault by considering the normal stress change. Our simulation results, which include no normal stress changes, also show the amplification at the hanging wall sites.

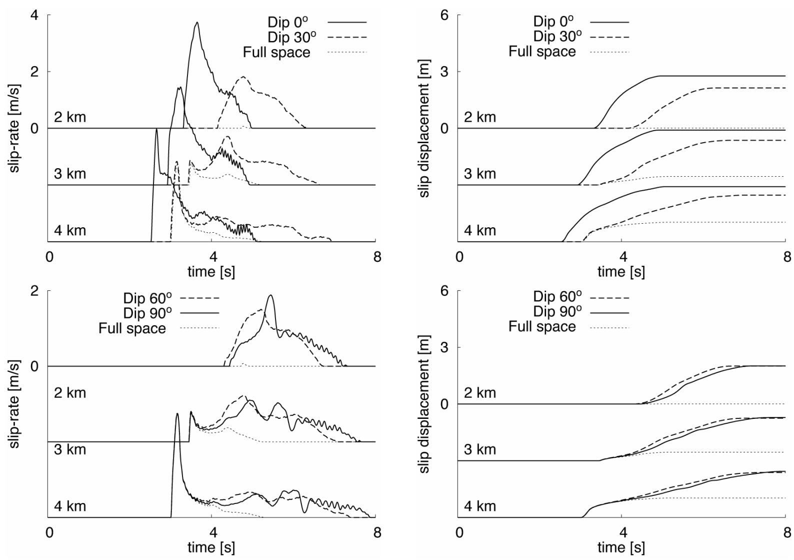

Figure 3 Slip-rate (left) and slip displacement (right) time histories

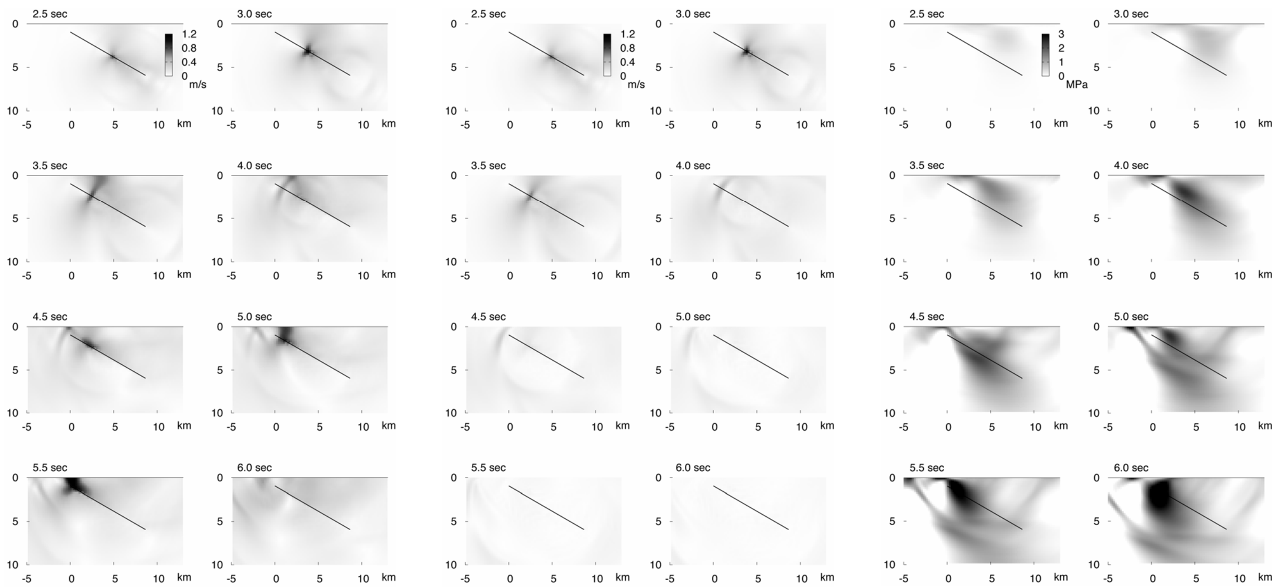

Figure 4 Snap shots of half space velocity field (left), full space velocity field (middle) and scattered Coulomb stress field (right) for Dip 30˚ case.

4. CONCLUSIONS

We proposed a combination approach of boundary integral equation method (BIEM) and finite element method (FEM). The key principles behind the proposed method are encapsulated in Eqn.2.9, which consists of 1) homogeneous full space solution calculated from BIEM, 2) FEM solution calculated in target inhomogeneous and/or bounded space, and 3) FEM solution calculated in homogeneous full space. Simple numerical simulations in a half space case indicate that some additional phases generated from the free surface, accelerate the rupture speeds and control the rupture generation.

The proposed approach takes advantage of the frameworks of each stand-alone BIEM and FEM, and allows one to use existing resources. Therefore, particular efficient techniques can be directly applied for the proposed approach, e.g. fast multipole method, adaptive mesh refinement, and parallel or grid computing schemes. We mention that whereas this approach offers the possibility of combining general boundary based methods and domain based methods, it requires that the boundaries or inhomogeneities be located away from the fault plane. Rupture simulation on the fault crossing the material boundary or located on a bi-material interface are future goals.

ACKNOWLEDGMENTS

This study was supported in part by Grant-in-Aid for Young Scientists Start-up of Japan Society for the Promotion of Science (JSPS) (HG). Two of us (LRG and JB) received funding from the National Science Foundation (NSF) under Grant Number ITR 0326449 Steve Meacham is the cognizant officer. We are grateful for this support.

REFERENCES

Aagaard, B. T. (1999). Finite-element simulations of earthquakes, Ph.D thesis.
Aki, K. and Richards, P. G. (2002). Quantitative Seismology 2nd edn, University Science Books, California.
Andrews, D. J. (1973). A numerical study of tectonic stress release by underground explosions, *Bull. seism. Soc. Am.*, **63**, 1375-1391.
Andrews, D. J. (1976). Rupture velocity of plane-strain shear cracks, *J. geophys. Res.*, **81**, 5679-5687.
Cochard, A. and Madariaga, R. (1994). Dynamic rupture faulting under rate-dependent friction, *Pure. Appl. Geophys.*, **142**, 419-445.
Cochard, A. and Rice, J. R. (1997). A spectral method for numerical elastodynamic fracture analysis without spatial replication of the rupture event, *J. Mech. Phys. Solids*, **45**, 1393-1418.
Cruz-Atienza, V. M. and Virieux, J. (2004). Dynamic rupture simulation of non-planar faults with a finitedifference approach, *Geophys. J Int.*, **158**, 939-954.
Dalguer, L. A. and Day S.M. (2006). Comparison of fault representation methods in finite difference simulations of dynamic rupture, *Bull. seism. Soc. Am.*, **96**, 1764-1778.
Dalguer, L. A. and Day, S.M. (2007). Staggered-grid split-node method for spontaneous rupture simulation, *J. geophys. Res.*, **112**, B02302.
Das, S. and Aki, K. (1977a). A numerical study of two-dimensional spontaneous rupture propagation, *Geophys. J. R. astr. Soc.*, **50**, 643-668.
Das, S. and Aki, K. (1977b). Fault plane with barriers: a versatile earthquake model, *J. geophys. Res.*, **82**, 5658-5670.
Das, S. (1980). A numerical method for the estimation of source time functions for general three-dimensional rupture propagation, *Geophys. J. R. astr. Soc.*, **62**, 591-604.
Day, S. M. (1982). Three-dimensional simulation of spontaneous rupture: the effect of nonuniform prestress, *Bull. seism. Soc. Am.*, **72**, 1881-1902.
Festa, D. G. (2004). Slip imaging by isochron back projection and source dynamics with spectral element methods, Ph.D. thesis.
Fukuyama, E. and Madariaga, R. (1995). Integral equation method for plane crack with arbitrary shape in 3D

elastic medium, *Bull. seism. Soc. Am.*, **85**, 614-628.
Fukuyama, E. and Madariaga, R. (1998). Rupture dynamics of a planar fault in a 3D elastic medium: rate- and slip-weakening friction, *Bull. seism. Soc. Am.*, **88**, 1-17.
Geubelle, P. H. and Rice, J. R. (1995). A spectral method for three-dimensional elastodynamic fracture problems, *J. Mech. Phys. Solids*, **43**, 1791-1824.
Goto, H. and Bielak, J. (2008). Galerkin boundary integral equation method for spontaneous rupture propagation problems: SH-case, *Geophys. J Int.*, **172**, 1083-1103.
Ida, Y. (1972). Cohesive force across the tip of a longitudinal-shear crack and Griffith's specific surface energy, *J. geophys. Res.*, **77**, 3796-3805.
Kase, Y. and Day, S. M., (2006). Spontaneous rupture propagation on a bending fault, *Geophys. Res. Lett.*, **33**, L10302.
Koller, M.G., Bonnet, M. and Madariaga, R. (1992). Modeling of dynamical crack propagation using timedomain boundary integral equations, *Wave Motion*, **16**, 339-366.
Kostrov, B. V. (1966). Unsteady propagation of longitudial shear cracks, *J. Appl. Math. Mech.*, **30**, 1241-1248.
Kostrov, B.V. and Das S. (1989). Principles of earthquake source mechanics, Cambridge University Press, Cambridge.
Lapusta, N., Rice, J. R., Ben-Zion, Y. and Zheng, G. (2000). Elastodynamic analysis for slow tectonic loading with spontaneous rupture episodes on faults with rate- and state-dependent friction, *J. geophys. Res.*, **105**, 23765-23789.
Madariaga, R., Olsen, K. B. and Archuleta, R. J. (1998). Modeling dynamic rupture in a 3D earthquake fault model, *Bull. seism. Soc. Am.*, **88**, 1182-1197.
Miyatake, T. and Kimura, T. (2006). Improvement in the fault boundary conditions for a staggered grid finitedifference method, *Pure Appl. Geophys*, **163**, 1977-1990.
Nishimura, N. and Kobayashi, S. (1989). A regularized boundary integral equation method for elastodynamic crack problems, *Comp. Mech.*, **4**, 319-328.
Oglesby, D. D. and Archuleta, R. J. (2000a). Dynamics of dip-slip faulting: explorations in two dimensions, *J. geophys. Res.*, **105**, 13643-13653.
Oglesby, D. D., Archuleta, R. J. and Nielsen, S. B. (2000b). The three-dimensional dynamics of dipping faults, *Bull. seism. Soc. Am.*, **90**, 616-628.
Sladek, V. and Sladek, J. (1984). Transient elastodynamic three-dimensional problems in cracked bodies, *Appl. Math. Modeling*, **8**, 2-10.
Tada, T. and Yamashita, T. (1997). Non-hypersingular boundary integral equations for two-dimensional nonplanar crack analysis, *Geophys. J Int.*, **130**, 269-282.
Tada, T., Fukuyama, E. and Madariaga, R. (2000). Non-hypersingular boundary integral equations for 3-D non-planar crack dynamics, *Comp. Mech.*, **25**, 613-626.
Zhang, H. and Chen, X. (2006a). Dynamic rupture on a planar fault in three-dimensional half space -I. Theory, *Geophys. J Int.*, **164**, 633-652.
Zhang, H. and Chen, X. (2006b). Dynamic rupture on a planar fault in three-dimensional half space -II. Validations and numerical experiments, *Geophys. J Int.*, **164**, 917-932.